ELSEVIER

Thermochimica Acta 306 (1997) 51–59

thermochimica acta

Temperature programmed reduction studies of nickel manganite spinels

Laberty Christel*, Alphonse Pierre, Duprat Anne-Marie Rousset Abel

Laboratoire de Chimie des Matériaux Inorganiques, 118 route de Narbonne 31062 Toulouse, Cedex, France

Received 19 February 1997; accepted 17 June 1997

Abstract

Temperature programmed reduction (TPR) of manganese, nickel monometallic oxides (Mn_3O_4, Mn_2O_3, MnO_2 and NiO) and nickel manganite oxides (spinels $Ni_xMn_{3-x}O_4$ with $0 < x \leq 1$ and ilmenite $NiMnO_3$), under hydrogen, was investigated. Final and transient products produced were characterised by XRD.

Manganese oxides are successively reduced to less oxidised oxide (MnO_2 gives Mn_2O_3 which gives Mn_3O_4 which further gives MnO). Although the position and shape of the peaks corresponding to the different reduction steps depend on experimental conditions and sample granulometry, activation energy is found to be the same for the same kind of transformation. Whatever is the crystalline structure, nickel manganites are reduced in two main steps. During the first step, formation of a solid solution of NiO in MnO matrix arises then reduction of Ni^{2+} cations occur during the last step and the final product of reaction is a mixture of MnO and metallic nickel. Hence, contrary to manganese oxides, Mn cations of mixed compounds undergo direct reduction to Mn^{2+}, giving MnO without any other way through less oxidised species of manganese. We think that it should be explained by the promoting effect of nickel. © 1997 Elsevier Science B.V.

Keywords: Manganese oxide; Nickel manganite; Nickel oxide; TPR

1. Introduction

Most mixed manganites $A_xMn_{3-x}O_4$ (A = Mg, Mn, Co, Zn, Ni) are normal spinels and have a cationic distribution: $A_x^{2+}Mn_{1-x}^{2+}[Mn^{3+}Mn^{3+}]O_4^{2-}$. Because of the strong preference of Ni^{2+} ions for octahedral sites, nickel manganites are inverse spinels with a cation arrangement: $Mn^{2+}[Ni_x^{2+}Mn_x^{4+}Mn_{2-2x}^{3+}]O_4^{2-}$. Occupation of octahedral sites by Ni^{2+} induces the existence of $Mn^{3+/4+}$ redox couples on the same lattice sites. These couples are the cause of the good electrical conductivity of nickel manganites (normal manganite spinels are all insulators) and these materials have been widely studied for thermistor ceramic applications [1,2]. For $x = 1$, the cationic distribution would be: $Mn^{2+}[Ni_x^{2+}Mn_x^{4+}Mn_{2-2x}^{3+}]O_4^{2-}$, but this arrangement does not account for the good conductivity of this oxide, which implies that a part of Ni^{2+} ions must be in tetrahedral sites. Moreover, some authors have proposed, from neutron diffraction studies, that tetrahedral sites also contain a small proportion of Mn^{3+} ions [3]. In order to clarify how the cation distribution changes when x varies, the initial aim of this work was to study these nickel manganites by temperature programmed reduction (TPR) technique.

Indeed, TPR is a highly sensitive technique for characterising solids and, although rather recent [4], it has been extensively applied to study the bulk and

*Corresponding author.

PII S0040-6031(97)00299-2

the surface of solid catalysts. Based on the measurement of reducibility of oxidised species, it allows the determination of the valence state of the cations and quantitative evaluation of the amount of nonstoichiometric oxygen both on the surface and in bulk [5,6]. The maximum temperature at which reduction takes place (T_m) is dependant of the heating rate (β) and activation energy of reduction can be calculated from some experimentally collected pairs of T_m and β values [7]. On the other hand, for a set of perovskite oxides, T_m have been correlated with catalytic activity for total CO oxidation [8,9] and also with oxygen binding energy [9].

In this paper, reduction of the bulk monometallic oxides NiO, MnO_2, Mn_2O_3, Mn_3O_4 has been first considered. The evolution of the reduction profile of mixed nickel manganites, according to nickel proportion, has been studied.

2. Experimental

2.1. Materials

Nickel oxide samples, labelled NiO(623) and NiO(1073), were prepared by thermal decomposition of nickel oxalate in air, for 4 h, at 623 or 1073 K. The oxalate was obtained by precipitation from aqueous solution of nickel nitrate with ammonium oxalate. After 1 h the precipitate was separated by filtration and washed with demineralised water.

MnO_2 oxides were commercial reagents: Merck No. 805958 and Ventron No. 89715.

Mn_2O_3 samples, labelled Mn_2O_3(793) and Mn_2O_3(1073), were synthesised by thermal decomposition of manganese oxalate in air, for 4 h, at 793 or 1073 K. Mn_3O_4 was synthesised by thermal decomposition of the manganese oxalate in air, for 4 h, at 1273 K. The manganese oxalate was obtained by precipitation from aqueous solution of manganese nitrate with ammonium oxalate.

The cubic spinels $Ni_xMn_{3-x}O_4$ with $0 < x < 1$ were prepared by the thermal decomposition, in air, of the mixed oxalate precursors, for 4 h, at 1173 K. Mixed manganese–nickel oxalates were obtained at room temperature by precipitation from aqueous solution of Mn^{2+} and Ni^{2+} nitrates with ammonium oxalate.

Table 1
BET specific surface area of oxides

Monometallic oxide	S ($m^2 g^{-1}$)	Mixed oxide	S ($m^2 g^{-1}$)
Mn_3O_4	0.2	$Ni_{0.2}Mn_{2.8}O_4$	0.3
Mn_2O_3(793)	22	$Ni_{0.4}Mn_{2.6}O_4$	0.4
Mn_2O_3(1073)	6	$Ni_{0.6}Mn_{2.4}O4$	0.6
MnO_2 Merck	61	$Ni_{0.8}Mn_{2.2}O_4$	0.9
MnO_2 Ventron	0.2	$NiMn_2O_4$	1.0
NiO(623)	100	$NiMnO_3$	6.3
NiO(1073)	15		

Ilmenite $NiMnO_3$ was prepared by thermal decomposition in air of suitable mixed oxalate precursor (Mn/Ni ratio = 1) at 973 K for 4 h.

2.2. Characterisation

The oxides were analysed by X-ray powder diffraction (XRD) with a Siemens diffractometer using CoK_α radiation. Specific surface areas were measured by nitrogen adsorption (BET method) using a Micromeritics Flowsorb 2300. The BET specific surface areas of different oxides are listed in Table 1. The chemical composition of the oxides was determined by means of atomic absorption spectroscopy.

2.3. Temperature programmed reduction (TPR)

TPR experiments were performed in a vertical plug flow differential reactor. The reaction was followed by thermogravimetric analysis using a Cahn D200 microbalance (accuracy 10^{-6} g). The carrier gas was a mixture of 10% H_2 in Ar with a flow rate of 20 cm^3 min^{-1}. The temperature of the samples was linearly increased by a furnace monitored by Shimaden SR25 temperature programmer. The amount of sample was usually 10.0 mg.

3. Results and discussion

3.1. Mn_3O_4

TPR of Mn_3O_4 has been already studied [13,14] because these oxides are used as selective reduction catalysts and it has been found that the activity and

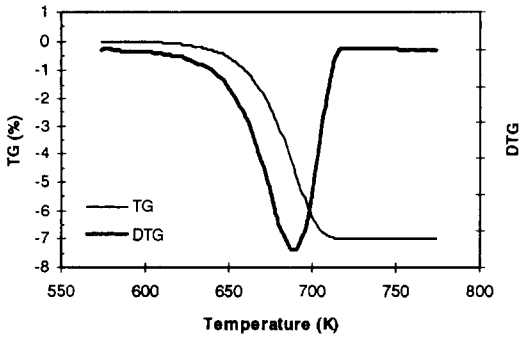

Fig. 1. TPR profiles (TG and DTG) of Mn_3O_4 1273 ($\beta = 0.033$ K s^{-1}).

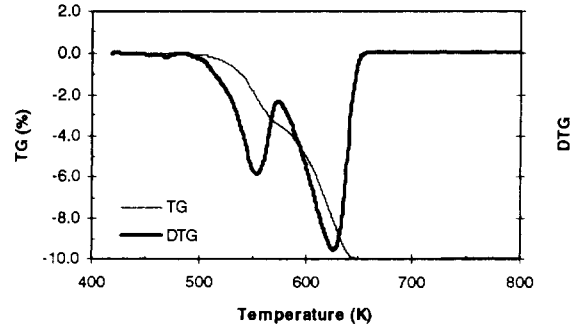

Fig. 2. TPR profiles (TG and DTG) of Mn_2O_3 793 ($\beta = 0.033$ K s^{-1}).

selectivity were in relation to the oxidation state of the catalysts.

Fig. 1 shows TPR profiles (TG and DTG) of the Mn_3O_4(1273) sample. Reduction occurs in one step. XRD analysis of the compound obtained after reduction reveals only the presence of MnO phase. Thus, the observed reaction is the reduction of Mn^{3+} to Mn^{2+} according to:

$$Mn_3O_4 + H_2 \rightarrow 3MnO + H_2O \quad (1)$$

On comparing the theoretical mass loss calculated from Eq. (1) with the experimental one (Table 2), we conclude that these oxides are stoichiometric. To evaluate the apparent activation energy (E_a) of the reaction we have measured the displacement of the maximum temperature at which reduction takes place (T_m) according to different heating rates (β) [7]. Since we work with a differential reactor (with very low fractional conversion), the value of E_a can be deduced from the slope of the line $\ln \beta/T_m^2 = f(1/T_m)$. A value of 97 kJ/mol (with a coefficient correlation $r^2 = 0.995$) was found.

Table 2
Mass loss observed for Mn_3O_4 reduction

Oxides	β (K s^{-1})	$\Delta m_{exp.}$ (%)	Δm_{calc} (%)	T_m (K)
Mn_3O_4	0.033	7.00	7.00	693
Mn_3O_4	0.083	7.00	7.00	731
Mn_3O_4	0.125	6.80	7.00	749
Mn_3O_4	0.167	6.90	7.00	757
Mn_3O_4	0.208	6.80	7.00	768

3.2. Mn_2O_3

Fig. 2 shows TPR profiles obtained for Mn_2O_3(793). Two reduction steps can be seen. XRD analysis of the compound formed after the first step reveals the presence of Mn_3O_4 and XRD pattern of the final product correspond to those of MnO. Hence,

- the first step corresponds to the reduction of Mn_2O_3 to Mn_3O_4 according to Eq. (2):

$$3Mn_2O_3 + H_2 \rightarrow 2Mn_3O_4 + H_2O \quad (2)$$

- the second step corresponds to the reduction of Mn_3O_4 to MnO according to Eq. (1).

Table 3 gives the theoretical (calculated from Eqs. (2) and (1)) and experimental mass loss averaged for several analyses. Experimental and calculated values are sufficiently similar to confirm that Mn_2O_3 reduction gives MnO via Mn_3O_4 formation. On comparing calculated and experimental mass loss for the total reaction we can conclude that this oxide is quite stoichiometric.

Table 3
Mass loss observed for Mn_2O_3 (793) reduction Δm (%)

	Δm (%) Step 1	Δm (%) Step 2	Δm (%) Total	β (K s^{-1})
Calculated	3.38	6.76	10.14	—
Experiment 1	3.38	6.57	9.98	0.03
Experiment 2	3.40	6.55	9.95	0.08
Experiment 3	3.50	6.70	10.20	0.13
Experiment 4	3.58	6.31	9.89	0.17

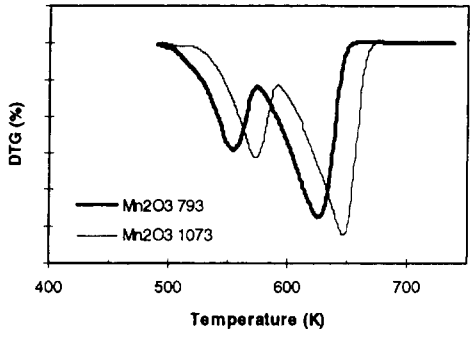

Fig. 3. TPR profiles (DTG) of Mn_2O_3 793 and Mn_2O_3 1073 ($\beta = 0.033$ K s^{-1}).

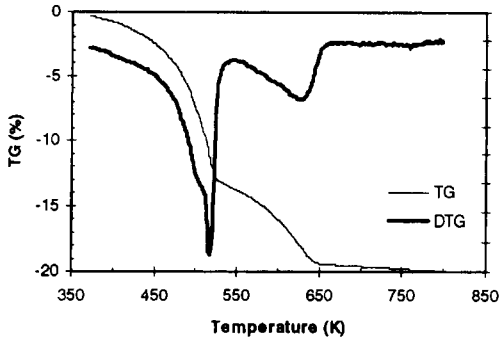

Fig. 4. TPR profiles (TG and DTG) of MnO_2 Merck ($\beta = 0.033$ K s^{-1}).

The comparison of TPR profiles (DTG) of Mn_2O_3(1073) and Mn_2O_3(793) shows (Fig. 3) a shift of Mn_2O_3(1073) curve of about 20 K towards high temperatures. This can be explained by the larger particle size of the oxide synthesised at 1073 K. Indeed, Mn_2O_3(1073) have specific surface area (6 m^2/g) almost four times less than Mn_2O_3(793) (22 m^2/g).

Several reduction experiments have been made on Mn_2O_3(1073) and Mn_2O_3(793) with different heating rate to determine the activation energy of both reduction steps (Table 4).

It appears that (i) E_a values are little dependent on particle size, (ii) activation energies of the two steps differ by about 10–15 kJ/mol, (iii) the energy found for the second step is rather similar to that previously observed for Mn_3O_4(1073) reduction of about 100 kJ/mol.

3.3. MnO_2

Fig. 4 shows the TPR profiles obtained for the reduction of MnO_2-Merck. Three successive reduction steps can be observed. XRD analysis of the compound formed after each step reveals the formation of Mn_2O_3 after the first stage, Mn_3O_4 after the second and MnO at the end of the reaction. Hence, MnO_2 is successively reduced according to Eqs. (1)–(3):

$$2MnO_2 + H_2 \rightarrow Mn_2O_3 + H_2O \quad (3)$$

Experimental and theoretical mass loss for each reduction stages, calculated from the above reactions, are summarised in Table 5. Experimental values are rather close to those calculated for steps 1 and 3; for the other stage the observed difference can probably be attributed to the poor separation between the two reduction processes (peak I appears only as a shoulder on peak II). On the other hand, the total mass loss observed is always greater than the expected one, hence these compound contain impurity probably hydroxyl group or water residues from the synthesis.

Fig. 5 shows the difference between the DTG curves of MnO_2-Merck and MnO_2-Ventron obtained for the same conditions of reduction. It can be noted that MnO_2-Ventron reduction occurs in only one stage at a temperature much above the Merck sample. This can be explained by the difference in particle size. Fig. 6 gives particle size distribution for both oxides. It appears that average particle size of MnO_2-Ventron particles is 100 times greater than the Merck oxide. This great difference agree well with the large gap

Table 4
Activation energies for reduction of Mn_2O_3(793) and Mn_2O_3(1073)

	Step one: $Mn_2O_3 \rightarrow Mn_3O_4$		Step two: $Mn_3O_4 \rightarrow MnO$	
	E_a (kJ/mol)	r^2	E_a (kJ/mol)	r^2
Mn_2O_3(793)	92±5	0.999	104±5	0.999
Mn_2O_3(1073)	85±5	0.993	98±5	0.991

Table 5
Mass loss observed for reduction of MnO_2

	β	Δm (%) Step 1	Δm (%) Step 2	Δm (%) Step 3	Δm (%) Total
Calculated	—	9.2	3.1	6.1	18.4
MnO_2 Merck	0.03	9.1	4.5	6.4	20.0
MnO_2 Merck	0.08	8.8	4.4	6.5	19.7
MnO_2 Merck	0.13	9.3	4.6	6.6	20.4
MnO_2 Merck	0.17	8.8	4.9	6.2	19.8
MnO_2 Ventron	0.08	17.6	—	—	17.6
MnO_2 Ventron	0.13	17.6	—	—	17.6
MnO_2 Ventron	0.17	17.1	—	—	17.1
MnO_2 Ventron	0.21	17.1	—	—	17.1

observed between specific surface areas of these oxides (60 $m^2 g^{-1}$ for MnO_2-Merck against 0.2 $m^2 g^{-1}$ for MnO_2-Ventron).

Values of the activation energy, for both samples, are reported in Table 6. In case of finely divided oxide, for the first step, that is the reduction of MnO_2 to Mn_2O_3, E_a is equal to 71 kJ mol^{-1}; the activation energies of the following steps are close to those previously observed for Mn_2O_3 and Mn_3O_4 reduction. For MnO_2-Ventron, only a single value of 86 kJ mol^{-1} was found.

3.4. NiO

TPR of nickel oxide has been widely studied [4,10–12]. This oxide has been used as a model for the study of the influence of different experimental operating variables [11] and particle size effects [12]. TPR profiles (DTG) of our two NiO samples, NiO(1073) and NiO(623), are shown in Fig. 7. Two main differences can be noted between these oxides: (i) the DTG curve of the low temperature compound presents three clearly defined peaks, whereas the reduction of NiO(1073) gives only an asymmetrical peak; (ii) there is a shift of about 100 K between the curves of the two samples; this temperature gap is in accordance with the great difference between the specific surface areas of these oxides: 100 $m^2 g^{-1}$ for NiO(623) against 15 $m^2 g^{-1}$ for NiO(1073). Experimental and calculated mass losses are reported in Table 7. Calculated values are computed from Eq. (4):

$$NiO + H_2 \rightarrow Ni + H_2O \quad (4)$$

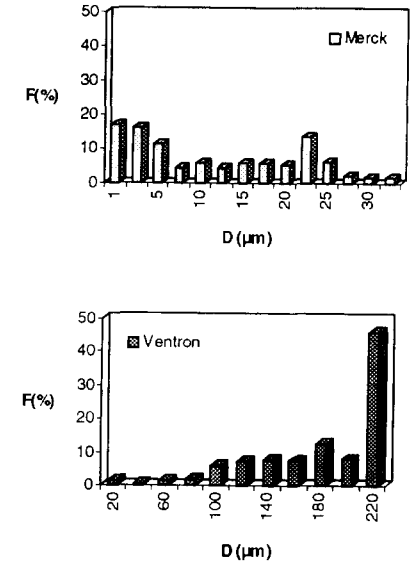

Fig. 6. Particle size distribution for MnO_2 Merck and MnO_2 Ventron.

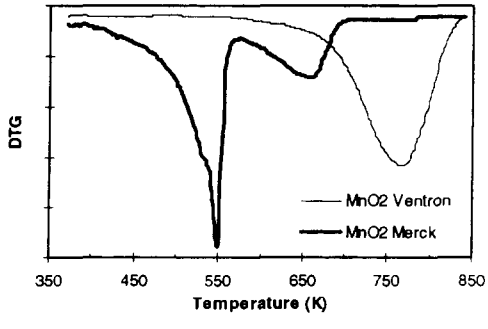

Fig. 5. TPR profiles (DTG) of MnO_2 Merck and MnO_2 Ventron ($\beta = 0.08$ K s^{-1}).

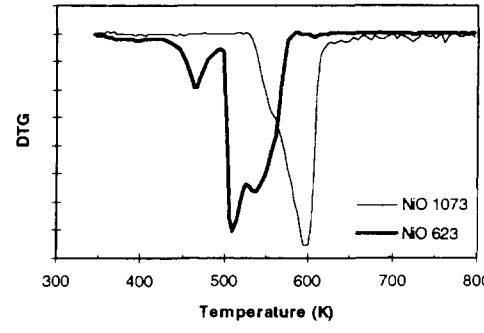

Fig. 7. TPR profiles (DTG) of NiO 1073 and NiO 623 ($\beta = 0.033$ K s^{-1}).

Table 6
Activation energies for reduction of MnO_2-Merck and MnO_2-Ventron

	Step 1		Step 2		Step 3	
	$MnO_2 \rightarrow Mn_2O_3$		$Mn_2O_3 \rightarrow Mn_3O_4$		$Mn_3O_4 \rightarrow MnO$	
	E_a (kJ/mol)	r^2	E_a (kJ/mol)	r^2	E_a (kJ/mol)	r^2
MnO_2-Merck	71	0.962	77	0.986	98	0.990
MnO_2-Ventron	85	0.998	—		—	

Table 7
Experimental and calculated mass loss for NiO reduction

Sample	β (°C/min)	Δm (%) experimental	Δm (%) calculated
NiO (1073)	2	21.9	21.4
NiO (1073)	5	21.3	21.4
NiO (1073)	7.5	20.9	21.4
NiO (1073)	10	21.2	21.4
NiO (623)	2	26.2	21.4
NiO (623)	2	26.3	21.4

For NiO(1073) the agreement between the measured and calculated values is rather satisfactory. This indicates that the final product of reduction is really the metallic nickel but also that NiO(1073) is stoichiometric. However, for NiO(623) a significant difference is observed between experimental and calculated values which imply that this oxide contains an excess of oxygen; indeed the chemical composition of this oxide will be: $NiO_{1.2}$.

The first step observed at about 450 K on TPR profile of NiO(623) corresponds to a mass loss of about 4%. Now if we calculate the mass loss for the reduction of nonstoichiometric nickel oxide $NiO_{1.2}$ to stoichiometric NiO, we will find 4.1%. Hence, we assume that the first step corresponds to the loss of nonstoichiometric oxygen, i.e. the reduction of Ni^{3+} cations to Ni^{2+}.

The other steps observed on TPR profiles of NiO(623) can probably be explained by mass transport limitations and/or particle size effects. Indeed, Fig. 8 demonstrates how TPR profiles are modified by preliminary grinding of sample. On comparing of the two particle size distributions reported on Fig. 9, we can suppose that the last two peaks observed on the TPR profile correspond to the successive reduction of two class of particles. In brief:

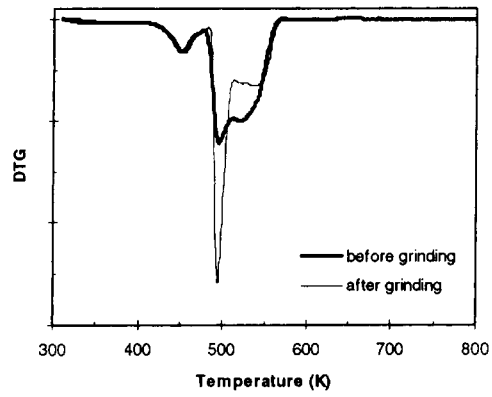

Fig. 8. Comparison between TPR profiles (DTG) of NiO 623 before and after grinding ($\beta = 0.033$ K s^{-1}).

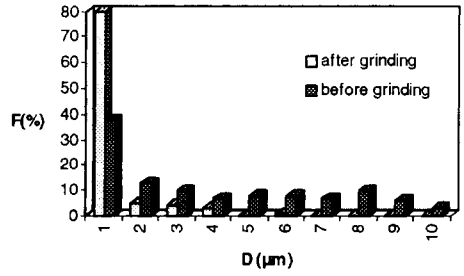

Fig. 9. Particle size distribution for NiO(623) before and after grinding.

(i) the low temperature peak is not affected by grinding, which confirm that it is due to the loss of nonstoichiometric oxygen (reduction of Ni^{3+} cations to Ni^{2+}).
(ii) the small particles (≤ 1 μm), whose population considerably increases by grinding, give the peak observed below 500 K.
(iii) the large particles (>1 μm), whose population is decreased by grinding, give the last peak.

On the other hand, values of the activation energy, found for NiO(1073) was 90 kJ/mol.

4. Nickel manganites

Fig. 10 shows the evolution of TPR profiles (DTG) of $Ni_xMn_{3-x}O_4$ when x increases from 0 to 1. As seen above, the reduction of the nickel free oxide (Mn_3O_4) occurs in only one step but when a part of the manganese is substituted by nickel the reduction proceed in two main stages. The first one occurs at low temperature (about 700 K) and gives a relatively sharp peak, sometimes having a shoulder ($Ni_{0.6}Mn_{2.4}O_4$). The second step takes place at higher temperature (950 K), giving one or more broad peaks.

The XRD spectra of the compound formed after the first step correspond to a solid solution of NiO in MnO (Fig. 11). XRD pattern of the product remaining after the reduction correspond to a mixture of MnO and metallic nickel.

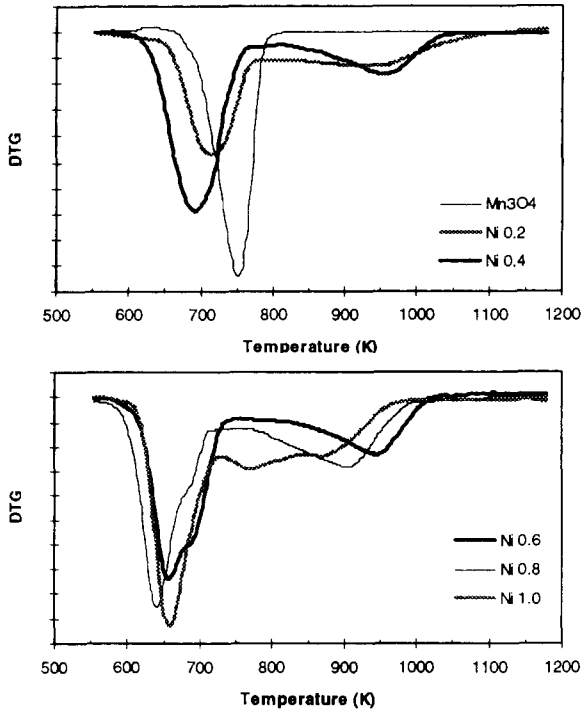

Fig. 10. Effect of nickel amount on TPR profile (DTG) of $Ni_xMn_{3-x}O_4$ ($\beta = 0.167$ K s^{-1}).

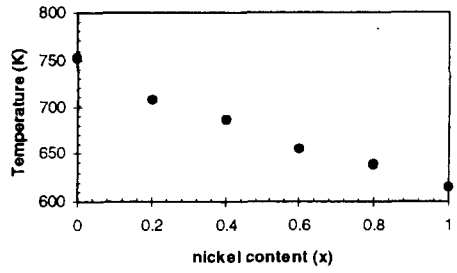

Fig. 11. Evolution with nickel content of the temperature maximum of the first TPR peak in $Ni_xMn_{3-x}O_4$ ($\beta = 0.167$ K s^{-1}).

In Table 8, the experimental and calculated mass losses are listed for different samples. Calculated mass losses are computed from reactions 5 and 6:

$$Ni_xMn_{3-x}O_4 + H_2 \rightarrow (3-x)MnO, xNiO + H_2O \quad (5)$$

$$(3-x)MnO, xNiO + xH_2 \rightarrow (3-x)MnO + xNi + xH_2O \quad (6)$$

Several points can be noted from the data listed in Table 8:

- mass loss (Δm) observed for the first step seems to be independent of nickel content of oxide;
- Δm corresponding to the second step increases with nickel content;
- experimental and calculated total mass loss are in good accordance, these indicate that these oxides were stoichiometric.
- experimental mass losses for the two steps are rather close to the calculated one from Eqs. (5) and (6).

Indeed, these results seem to show that, during the first stage of the reduction, the major part of the manganese cations are reduced to Mn^{2+}, giving a solid solution of NiO in MnO, according to Eq. (5). Then reduction of Ni^{2+} cations to MnO matrix occurs during the last step, according to reaction 6.

In Fig. 11, the maximum temperature of the first peak is plotted against the nickel content (x). It is clear that more the nickel amount increases, easier the reduction becomes. Based on previous works, this can be explained in terms of a promoting effect of nickel which can result from two processes: (i) nickel metal atoms form sites for the adsorption of hydrogen, this lead to enhanced concentrations of surface hydrogen via a spillover mechanism [15–17]; (ii) the pre-

Table 8
Experimental and calculated mass loss for reduction of $Ni_xMn_{3-x}O_4$

x	Δm (%) Step 1	Δm (%) Step 2	Δm (%) Total	Δm (%) Total calculated	Δm (%) Mn reduction	Δm (%) Ni reduction
0	7.0	0.0	7.0	7.0	7.0	0.0
0.2	6.7	2.0	8.7	8.4	7.0	1.4
0.4	6.9	3.2	10.1	9.7	6.9	2.8
0.6	6.7	4.4	11.2	11.1	6.9	4.2
0.8	6.7	6.1	12.8	12.4	6.9	5.5
1.0	7.0	6.9	13.9	13.8	6.9	6.9

sence of nickel in the lattice directly increases the number of nucleation sites [18,19].

In our case, two reasons are in favour of a promoting effect due to increased nucleation sites:

- several reduction experiments, with different heating rate, have allowed us to determine activation energy of the first reduction step in $NiMn_2O_4$. It is found to be equal to 75 kJ/mol ($r^2 = 0.99$). So, the presence of nickel does not significantly decrease the activation energy for the reduction of manganese cations (70 kJ/mol for $Mn^{4+} \rightarrow Mn^{3+}$ and 90 kJ/mol for $Mn^{3+} \rightarrow Mn^{2+}$). Consequently, it is unlikely that promoting influence arises from molecular hydrogen activation.
- comparison between TPR profiles of MnO_2 (Fig. 7) and NiO (Fig. 8) seems to indicate that Mn^{4+} undergoes a reduction at lower temperature than Ni^{2+} and therefore the formation of metallic nickel during the first stage of the reaction is rather improbable.

It can be noticed from Fig. 10 that, except for $Ni_{0.6}Mn_{2.4}O_4$, the low temperature stage of reduction gives only one peak. Since this stage have been assigned to the reduction of manganese cation in Mn^{2+} and there are two kinds of high valence manganese cation in nickel manganite (Mn^{3+} and Mn^{4+}), several separate reduction steps would be expected as above for the monometallic manganese oxides. On the other hand, why several peaks are present on the TPR profiles corresponding to the high temperature stage of reduction although only one specie (Ni^{2+}) is reduced during this stage?

We think that the impossibility of separating the transient states of manganese reduction is mainly due to the activating effect of nickel which causes direct reduction of Mn^{4+} or Mn^{3+} in Mn^{2+}. On the other hand, the additional peaks observed, for the first step with $Ni_{0.6}Mn_{2.4}O_4$, or in the last step with nickel rich oxides, can be explained by particle size effects and/or mass transport limitations as shown in Fig. 12.

In order to verify whether the similar behaviour could be observed with another nickel manganite, which does not have the spinel structure, we have studied the TPR of $NiMnO_3$. In this compound, which has an ilmenite structure, manganese is present only as Mn^{4+} state. Fig. 13 shows the TPR profiles obtained for the reduction of $NiMnO_3$. As with spinel oxides, the reaction proceeds in two steps, the first giving a sharp peak and the second a broad one. In Table 9, the experimental and calculated mass loss are listed for several experiments. Calculated mass loss are computed by assuming that during the first step all Mn^{4+} cations are reduced to Mn^{2+}, the second step corresponded to Ni^{2+} reduction in metallic nickel. It can be seen that the experimental values agree well with the calculated one for step 2, although for step 1 experimental values are systematically less than the expected. This could be explained by the fact that a part of the Mn cations are indeed under Mn^{3+} state;

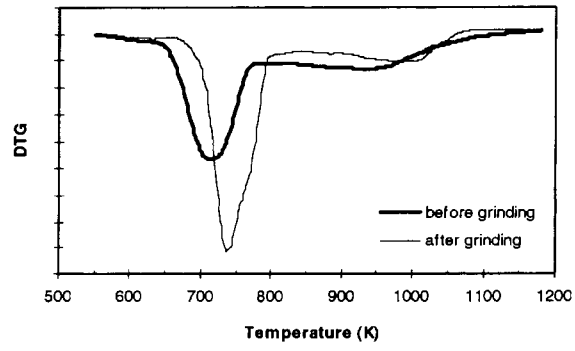

Fig. 12. Influence of preliminary grinding on TPR profile (DTG) of $Ni_{0.2}Mn_{2.8}O_4$ ($\beta = 0.167$ K s^{-1}).

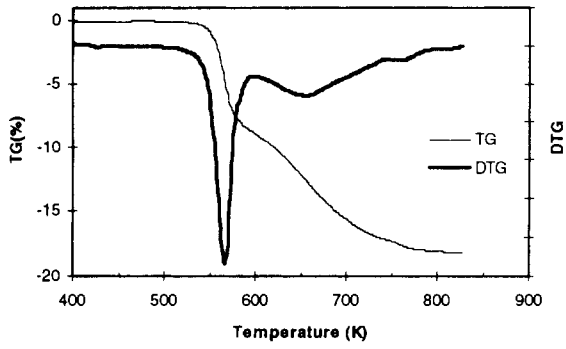

Fig. 13. TPR profiles (TG and DTG) of $NiMnO_3$ ($\beta = 0.033\ K\ s^{-1}$).

Table 9
Experimental and calculated mass loss for reduction of $NiMnO_3$

	Δm (%) Step 1	Δm (%) Step 2	Δm (%) Total	β ($K\ s^{-1}$)
Calculated	9.9	9.9	19.8	—
Experiment 1	8.6	9.6	18.2	0.03
Experiment 2	8.4	9.7	18.1	0.08
Experiment 3	8.4	9.8	18.2	0.13
Experiment 4	8.7	9.7	18.4	0.17
Experiment 5	8.1	9.7	17.8	0.21

indeed enhanced XRD analysis confirms that this oxide is not pure $NiMnO_3$ but also contains a small amount of Mn_2O_3.

The determination of the apparent activation energy from the different heating rate reduction experiments gives 76 kJ/mol for the first reduction step of $NiMnO_3$. This value is very close to the observed value for the spinel oxide.

In brief, TPR of $NiMnO_3$ confirms that, in mixed nickel manganese oxides, promoting effect of nickel prevent the reaction going through the less oxidised state of manganese cations.

5. Conclusion

TPR studies of different manganese oxides under hydrogen show that these compounds are successively reduced in less oxidised oxide (MnO_2 gives Mn_2O_3 which gives Mn_3O_4 which lastly gives MnO). Whatever the initial oxide, the apparent activation energy is found to be the same for the same reduction process.

Reduction of nickel manganite spinels proceeds in two main steps. During the first, the major part of manganese cations are reduced in Mn^{2+}, giving a solid solution of NiO in MnO, then reduction of Ni^{2+} cations in the MnO matrix occurs during the last step and the final product of reaction is a mixture of MnO and metallic nickel. Even with varying heating rates we do not succeed in detecting, during the first step, a way through less oxidised state of manganese. Hence, our initial goal, using TPR for cation distribution determination in nickel manganite spinels, was revealed ineffectual because, contrary to manganese oxides, Mn^{4+} and Mn^{3+} cations directly undergo reduction to Mn^{2+} giving MnO. This can be explained by a promoting effect of nickel, which accelerate the reaction process probably by increasing the number of nucleation sites.

References

[1] E. Jabry, G. Boissier, A. Rousset, P. Carnet and A. Lagrange, J. Phys. Science of ceramics 13, P. Odier, F. Cabannes, B. Calos (Eds.), C1, 1986, p. 843.
[2] R. Legros, R. Metz, A. Rousset, J. Mater. Sc. 25 (1990) 4410.
[3] J.L. Baudour, F. Bouree, M.A. Fremy, R. Legros, A. Rousset, B. Gillot, Physica B. 180 (1992) 97–99.
[4] S.D. Robertson, B.D. Mc Nicol, J.H. de Bass, S.C. Kloet, J.W. Jenkins, J. Catal. 37 (1975) 424.
[5] M.L. Rojas, J.L.G. Fierro, L.G. Tejuca, A.T. Bell, J. Catal. 124 (1990) 41–51.
[6] N.K. Kotsev, L.I. Llieva, Catalysis Letters 8 (1993) 173–176.
[7] H.E. Kissinger, J. of Research of the National Bureau of Standards, 57(4) (1956) 217.
[8] J.L.G. Fierro, J.M.D. Tarascon, L.G. Tejuca, J. Catal. 89 (1984) 209–216.
[9] M. Futaiu, C. Yonghua, L. Hangzhou, React. Kinet. Catal. Lett. 31 (1986) 35–47.
[10] R. Brown, M.E. Cooper, D.A. Whan, Appl. Catal. 3 (1982) 177.
[11] D.A. Monti, A. Baker, J. Catal. 83 (1983) 323.
[12] K.H. Tonge, Thermochimica Acta 74 (1984) 151–166.
[13] A. Maltha, T.L.F. Favre, H.F. Kist, A.P. Zuur, V. Ponec, J. Catal. 149 (1994) 149.
[14] Y. Yang, R. Huang, L. Chen, J. Zhang, Appl. Catal. (A) 101 (1993) 233.
[15] A. Roman and B. Delmon, C.R. Acad. Sc. Paris, 273, C, (1971) 94.
[16] H. Charcosset, B. Delmon, Ind. Chim. Belg. 38 (1973) 481.
[17] J.M. Zabala, P. Grange, and B. Delmon, C.R. Acad. Sc., Paris, 279, serie C, (1974) 561.
[18] S.J. Gentry, N.W. Hurst, A. Jones, J. Chem. Soc. Faraday Trans. 77 (1981) 603.
[19] A. Jones, B. Mc Nicol, Temperature Programmed Reduction for Solid Materials Characterization, M. Dekker (Ed.), 1986, p. 32.